



Catalytic C–O bond hydrogenolysis of tetrahydrofuran-dimethanol over metal supported WO_x/TiO_2 catalysts



Jiayue He^a, Samuel P. Burt^{a,b}, Madelyn R. Ball^a, Ive Hermans^{a,b}, James A. Dumesic^a, George W. Huber^{a,*}

^a Department of Chemical and Biological Engineering, University of Wisconsin-Madison, Madison, WI 53706, USA

^b Department of Chemistry, University of Wisconsin-Madison, Madison, WI 53706, USA

ARTICLE INFO

Keywords:

Biochemicals
Biomass
1,6-hexanediol
Catalyst

ABSTRACT

$\text{M-WO}_x/\text{TiO}_2$ ($\text{M} = \text{Pt-}, \text{Rh-}, \text{Pd-}, \text{and Ru}$) catalysts were prepared and studied for tetrahydrofuran-dimethanol (THFDM) hydrogenolysis. All catalysts have a small metal particle size ($< 2 \text{ nm}$) but show catalytic activities that differ by two orders of magnitude. From a combination of CO chemisorption and STEM, we conclude that this wide gap in activity is primarily due to overgrowth of WO_x/TiO_2 covering the metal particle of the less-active catalysts. This overgrowth decreases the number of exposed hydrogenation sites in these catalysts, lowering the overall reaction rate. The catalyst with the highest activity ($\text{Pt-WO}_x/\text{TiO}_2$) was studied at various pressures of H_2 , with catalytic activity passing through a maximum with increasing pressure. This is likely due to changes in the oxidation state of W^{8+} on the catalyst surface, which changes from W^{6+} to W^{5+} and W^{4+} with increasing hydrogen pressure. Moreover, H_2 can strongly adsorb on the catalyst surface and inhibit the activity at high hydrogen pressure. The apparent activation energy of THFDM conversion over $\text{Pt-WO}_x/\text{TiO}_2$ is 47 kJ mol^{-1} . $\text{Pt-WO}_x/\text{TiO}_2$ showed a decrease in conversion from 45% to 23% over 46 h on stream in a continuous flow reactor. Catalyst deactivation is likely due to leaching of W. THFDM can be efficiently converted to 1,2,6-hexanetriol (HTO) in the presence of Pt/TiO_2 and homogeneous W salts.

1. Introduction

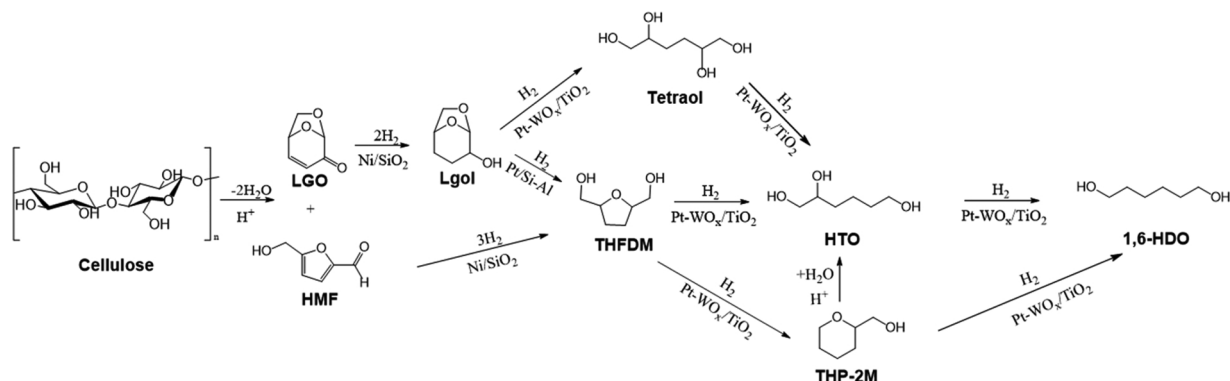
Cellulose derived from lignocellulosic biomass is the most abundant renewable carbon resource in nature, making it a promising feedstock for the production of bio-based chemicals [1–5]. 1,6-Hexanediol (1,6-HDO) is a high value chemical with a market price of \$4,400/ton, an annual market size of 138,000 tons, and a global market value of approximately \$600 MM [6]. It is primarily used as a monomer for polyesters and polyurethanes [7]. The most common industrial route for 1,6-HDO production begins with naphtha cracking to benzene, which is then hydrogenated to cyclohexane, which can be oxidized to a mixture of cyclohexanol and cyclohexanone (KA oil) [8,9]. KA oil can then be further oxidized to adipic acid or its esters, which are finally hydrogenated to 1,6-HDO [7–11]. This traditional route suffers from low single pass conversions, homogeneous chemistry, excess use of HNO_3 which leads to the production of N_xO_y , and the nonrenewable use of petroleum-based feedstocks. It would be desirable to develop a new route to 1,6-HDO from renewable lignocellulosic feedstocks.

Several academic and industrial groups have studied the production of 1,6-HDO from cellulose-derived feedstocks. Each route studied

appears to pass through the common intermediate tetrahydrofuran-dimethanol (THFDM) [12]. Hydrogenolysis of THFDM to 1,6-HDO, therefore, is of importance to the production of 1,6-HDO from cellulose. In 1981, Faber showed THFDM hydrogenolysis over a copper chromite catalyst, but 1,6-HDO yields were not reported [13]. Buntara *et al.* reported a one-pot conversion of THFDM to 1,6-HDO using a combination of $\text{Rh-ReO}_x/\text{SiO}_2$ and Nafion SAC-13 with 1,6-HDO yields up to 86% [14,15]. This process suffers from low catalyst activity ($0.10 \text{ mol mol}_{\text{Rh}}^{-1} \text{ min}^{-1}$ with THFDM conversion of 21% at 80°C) and rapid catalyst deactivation, primarily due to high solubility of the SiO_2 support in the solvent, water [14,15]. Rh-ReO_x , as well as base metal catalysts, have been extensively studied for the conversion of tetrahydropyran-2-methanol (THP-2 M) to 1,6-HDO [16–18], but they have not been shown to be active for the one-step conversion of THFDM to 1,6-HDO. As shown previously and again here in **Scheme 1**, THP-2 M is an intermediate between THFDM and 1,6-HDO [12]. Most recently, Rennovia, Dupont, and our group have reported a process to convert THFDM to 1,6-HDO over a $\text{Pt-WO}_x/\text{TiO}_2$ catalyst with 1,6-HDO yields over 70% [12,19,20]. Using a combination of Raman spectroscopy, X-ray Photoelectron Spectroscopy (XPS), and CO chemisorption, it was

* Corresponding author.

E-mail address: gwhuber@wisc.edu (G.W. Huber).



Scheme 1. Proposed reaction pathway for the conversion of cellulose derived oxygenates. [12,25–29].

determined that H₂ spillover from the Pt nanoparticle to WO_x was effective in reducing W⁶⁺ to W⁵⁺, generating a Brønsted acid site that is active for activation of the C–O bond to open the ring of THFDM [12]. This spillover was possible even in the absence of direct contact between WO_x and Pt, due to the reducible nature of TiO₂ facilitating H atom transfer over the catalyst surface over distances on the order of micrometers from the Pt particle [12,21].

In our previous paper, we showed that the role of Pt was to dissociate H₂ and provide hydrogenation sites [12]. The objective of this paper is to investigate the role of different noble metals, H₂ pressure, reaction temperature, and homogeneous tungsten salts on THFDM hydrogenolysis. We have also observed that the TOF of 10 wt.% Pt-WO_x/TiO₂ are higher than the TOF of 4 wt.% Pt-WO_x/TiO₂. Therefore, a 10 wt.% Pt is used in this study [12]. We first investigate whether this high reactivity for THFDM hydrogenolysis is specific to Pt-WO_x/TiO₂ or if other metals commonly used for hydrogenations (Rh, Pd, Ru) can be substituted for Pt as a hydrogenation catalyst, while maintaining similar reactivity or even improving it [22–24]. We then use XPS, STEM, and CO chemisorption to investigate the cause for the reactivity trends we see in these catalysts. Next, we study the effect of temperature on reactivity, and calculate an activation energy for THFDM conversion. We use XPS to help explain our reactivity trends. We then study the most active catalyst in a fixed-bed reactor and investigate causes of deactivation.

2. Experimental

2.1. Catalytic reactions

2.1.1. THFDM conversion in a batch reactor

Reactions were performed in 50 mL HEL high-pressure batch reactors. Prior to reactions, the catalysts were activated under flowing H₂ (100 mL (STP) min⁻¹) (Airgas, UHP) at 250 °C for two hours (1 °C min⁻¹). The reactant solution in water (Fisher Scientific #11307090) was prepared and then pumped into the reactor. During aqueous solution preparation, the insoluble impurities were removed by filtration with 0.22 μm PES (polyethersulfone) syringe filter. The reactor was purged three times with H₂ prior to reaction, pressurized to the desired H₂ pressure, stirred at 700 rpm, and heated to the reaction temperature. After reaction, the reactor was cooled in ice water and depressurized. The effect of the stirring rate was carefully evaluated. It is found that the reaction rates/conversions are the same when the stirring rate is above 600 rpm. Therefore, there are no external transport limitations under our reaction conditions (700 rpm). The product mixture was then filtered using a 0.22 μm PES syringe filter.

Products were quantified with a Shimadzu Gas Chromatograph using a Flame Ionization Detector (FID) with liquid injection. A Restek RTX-VMS capillary column (Length: 30 m, ID: 0.25 mm, film thickness: 1.4 μm) was used. The FID response factor of unknown products with

retention times close to that of 1,2-hexanediol (1,2-HDO) was assumed to be equal to that of 1,2-HDO. Based on this assumption, the carbon balance was calculated to be 95% ± 5% in all experiments.

2.1.2. THFDM conversion in continuous flow reactor for stability test

Hydrogenolysis was carried out in a grade 316 stainless-steel tubular flow reactor (30 cm long, 6.35 mm outer diameter) arranged in an upflow configuration and heated using a tube furnace (Thermcraft Inc. No. 114-12-1ZH). The catalyst (0.10 g), without dilution, was added into the reactor with quartz wool and quartz beads packed on both sides. The catalyst without dilution was reduced under a H₂ flow (100 mL (STP) min⁻¹) at 250 °C for 2 h before reaction. The reactor was cooled to 160 °C and pressurized to 3.4 MPa H₂. An aqueous 1 wt% THFDM solution was pumped into the reactor at 0.04 mL/min using an Agilent Prostar HPLC pump with co-fed H₂ (40 mL (STP) min⁻¹). Two stainless steel tanks (150 mL each) were used to accumulate the liquid products at the reactor outlet. The accumulated liquid product was drained periodically into a collector container, filtered through a 0.22 μm PES syringe filter, and then analyzed by GC. The carbon balance in the first 10 h was poor, indicating that this time was required to achieve steady state, therefore data is only reported after 10 h time on stream. The gaseous products continued to flow through a back-pressure regulator to maintain the reaction pressure. Both an excess flow shut-off valve and a pressure relief valve were also installed in the reactor system to ensure safe operation. The feed solutions and the liquid products were analyzed using a gas chromatograph (Shimadzu, GC-2010) equipped with a FID and a Restek RTX-VMS capillary column. The gas effluent from the continuous flow reactor was analyzed using a gas chromatograph (Shimadzu, GC-2014) equipped with an FID and a Restek RT-Q-Bond capillary column as well as a thermal conductivity detector and a ShinCarbon ST micropacked column.

2.2. Catalyst synthesis

2.2.1. WO_x/TiO₂ supports synthesis

WO_x/TiO₂ supports was synthesized by wet impregnation of ammonium tungsten oxide hydrate (Alfa Aesar #22640) on TiO₂ nanopowder (Sigma-Aldrich #718467). Ammonium tungsten oxide hydrate was first added to 100 mL of 18 MΩ water. To dissolve the tungsten precursor, HCl (Sigma-Aldrich #258148) was added dropwise to the mixture until it reached a pH of 1, and the mixture was then heated under reflux to 80 °C for 12 h. 6 g of TiO₂ nanopowder were then added to the mixture and left to stir for an additional 30 min at 80 °C. Water was then evaporated by rotary evaporation using a water bath at 60 °C. WO_x/TiO₂ powders were then dried at 110 °C overnight and calcined under flowing air at 400 °C for three hours (1 °C min⁻¹).

2.2.2. M-WO_x/TiO₂ and M/TiO₂ catalysts synthesis

All the catalysts were synthesized with similar procedures. For

example, Pt-WO_x/TiO₂ catalysts were synthesized by wet impregnation of chloroplatinic acid (Sigma-Aldrich #262587) on synthesized WO_x/TiO₂ and TiO₂ supports. (The precursors for Ru-, Rh-, and Pd-WO_x/TiO₂ are ruthenium (III) chloride (Sigma-Aldrich #208523), rhodium (III) nitrate hydrate (Sigma-Aldrich #83750) and palladium (II) nitrate dihydrate (Sigma-Aldrich #76070), respectively.) A chloroplatinic acid solution in water was added to the WO_x/TiO₂ support. The mixture was then heated to 80 °C while stirring. The mixture was then dried at 80 °C in vacuum oven overnight. The dry solid was ground to a powder. The powder was then calcined under flowing air (Airgas, UHP, 100 mL min⁻¹) at 400 °C for three hours (1 °C min⁻¹) and subsequently reduced under flowing H₂ (Airgas, UHP, 100 mL (STP) min⁻¹) at 250 °C for two hours (1 °C min⁻¹). After cooling to room temperature, the catalysts were passivated under flowing 1% air in He (Airgas, UHP) or transferred and stored in a glovebox.

2.3. Catalyst characterization

2.3.1. Inductively coupled plasma-atomic emission spectroscopy (ICP-AES)

The solid samples were digested in a mixture of HCl (Sigma-Aldrich #258148), HNO₃ (Sigma-Aldrich #438073), and HF (Sigma-Aldrich #339261) at 120 °C overnight. The elemental compositions of the synthesized samples were analyzed by ICP-OES (Varian Vista-MPX CCD Simultaneous ICP-OES). Metal standards for the ICP analysis were prepared from Fluka (1000 ± 2 mg/L).

2.3.2. N₂ physisorption measurements

N₂ physisorption measurements were measured on a Micromeritics 3Flex apparatus. The samples were degassed prior to measurement for 4 h at 150 °C under vacuum. Adsorption isotherms were collected at -196.15 °C and analyzed using the BET method.

2.3.3. X-ray photoelectron spectroscopy (XPS)

Surface compositions were characterized by XPS using a K-alpha XPS (Thermo Scientific) instrument with a micro-focused monochromatic Al K α X-ray source. Prior to analysis, the catalysts were reduced with flowing H₂ at 250 °C for two hours (1 °C min⁻¹), and stored in an oxygen-free environment, where they could be loaded in an air-tight sample holder for transport to the spectrometer. When it was desired to analyze oxidized samples, catalysts were treated in 1% O₂/N₂ at room temperature after reduction, and the same process was carried out. The samples were analyzed at 10⁻⁷ mbar pressure and room temperature. The spectra in the C1s, O1s, Pt4f, W4d, and Ti2p regions were collected over multiple scans; the number of scans was adjusted for each element (C = 15, O = 20, Pt = 60, W = 60, Ti = 20) to obtain an acceptable signal/noise ratio. The pass energy was held at 50 eV, the dwell time at 50 ms, and the energy step size at 0.2 eV for each region. Each region was integrated using the Avantage (Thermo Scientific) software package for determination of surface composition.

2.3.4. CO chemisorption

CO Chemisorption measurements were carried out with a Micromeritics Autochem II Chemisorption Analyzer. Approximately 100 mg of sample was used for each measurement. Prior to CO chemisorption, samples were reduced under 40 mL (STP) min⁻¹ 10%H₂/Ar (Airgas) to 250 °C (1 °C min⁻¹) for two hours. Samples were then cooled to 35 °C under 10 mL (STP) min⁻¹ He (Airgas, UHP) flow. 5%CO/He (Airgas) was then pulsed onto the catalyst in 0.5 mL (STP) increments until consecutive signals were equal. Signals were then integrated to determine total CO consumption.

2.4. THFDM synthesis

5-(hydroxymethyl) furfural (HMF, Hefei Leaf Biotech, 12.0 g), the solvent (120 mL ethanol, Decon Laboratories, INC.) and Ni/SiO₂ (64 wt. %, Strem #28-1900, 1.20 g) were added to a 300 mL Hastalloy Parr

autoclave. The reactor was flushed three times with hydrogen and pressurized to 8 MPa. The reaction mixture was stirred at 700 rpm and heated to 80 °C for 6 h. The autoclave was then allowed to cool to ambient temperature and the pressure was released. The obtained mixture was first filtered with a 0.22 µm PTFE (polytetrafluoroethylene) syringe filter to remove Ni/SiO₂. The solvent ethanol was evaporated with rotary evaporation using a water bath of 80 °C. The obtained liquid (THFDM) was analyzed by GC and ¹³C NMR (Fig. S4).

The product from HMF hydrogenation was characterized with ¹³C NMR. The sample was rotary evaporated to remove the ethanol solvent and dissolved in D₂O. The NMR experiments were carried out using a Bruker Biospin (Billerica, MA) AVANCE III 500 MHz spectrometer fitted with a DCH (¹³C-Optimized cyroprobe). The ¹³C experiments were run with the Bruker standard pulse sequence 'zgig30' with 128 scans of 65,786 data points at a 1 s acquisition time, a 12 s inter-scan relaxation delay, and a 262 ppm sweep width centered at 100 ppm. MestReNova software was used to process the spectra and the spectra were referenced to the residual water peak at 4.79 ppm.

3. Results and discussion

3.1. THFDM conversion over M-WO_x/TiO₂ catalysts

Fig. 1 shows the product distribution for THFDM conversion over the four bimetallic catalysts used in this study. Figs. 1a and b show that Ru- and Pd-WO_x/TiO₂ exhibit low activity for this reaction, whereas the Pt and Rh-WO_x/TiO₂ have higher activities. This behavior is similar to the study of Amada *et al.*, who observed that Pd-ReO_x/SiO₂ exhibits almost no activity for glycerol hydrogenolysis at 100 °C [30]. Tomishige *et al.* also reported that the promoting effect of oxophilic Re on Ru is different from the effect of Re on Rh or Ir [31]. The oxophilic additive can, in some cases, cover the metal nanoparticle, thereby decreasing activity of the bimetallic catalyst [32]. Fig. 1 indicates that this behavior could be the case for Pd- and Ru-WO_x/TiO₂, which will be discussed in more detail later. Fig. 1 shows that Ru- and Pt-WO_x/TiO₂ exhibit > 98% selectivity to 1,2,6-hexanetriol (HTO), which can then be selectively converted to 1,6-HDO, as shown in our previous paper [12]. Rh-WO_x/TiO₂ displays 80–85% HTO selectivity with THP-2 M as the main byproduct [16,17,32]. Pd-WO_x/TiO₂ shows less than 40% selectivity to HTO. However, this catalyst achieves a combined selectivity of ~80% to 1,6-HDO and its precursors.

Fig. 2 shows STEM images of Pt-, Rh-, Pd-, and Ru-WO_x/TiO₂ catalysts prepared in this study. STEM images of monometallic catalysts can be found in the supporting information (Fig. S1). The average metal particle sizes of the Pt, Rh, and Pd catalysts range from 1.45 to 1.74 nm. Ru-WO_x/TiO₂ has a smaller average particle size of 0.63 nm. These small particles are typical for noble metals and align with other reported metal-tungsten catalysts in the literature [33–39]. Such high loading metal catalysts have been reported to have larger particles, however, particles are usually smaller than 5 nm for these noble metals [40]. Table 1 shows average particle sizes determined by STEM, along with CO uptake, CO uptake derived particle sizes, and TOFs for THFDM conversion. The particle sizes determined by STEM of Pt-, Rh-, Ru-, Pd-WO_x/TiO₂ are smaller than the particle size calculated from CO chemisorption, particularly for the Pd and Ru catalysts (Entry 1–4, Table 1). Since CO does not adsorb on WO_x/TiO₂, this indicates that the noble metal particles may be overcoated by WO_x to some extent. There is a monolayer of WO_x (around 10 wt% loading) on TiO₂ surface (Scheme S1) since WO_x/TiO₂ is synthesized by first impregnating WO_x on TiO₂. The Pt is then impregnated on WO_x/TiO₂, so there is likely little contact between metal nanoparticles and TiO₂. Pd- and Ru-WO_x/TiO₂ (36 and 5 µmol g⁻¹) have less than half of the CO uptake as Pt-(85 µmol g⁻¹) and Rh-WO_x/TiO₂ (99 µmol g⁻¹), even though STEM images show that Pd-(1.45 ± 1.53 nm) and Ru-WO_x/TiO₂ (0.63 ± 0.66 nm) have similar average particle sizes to the other two

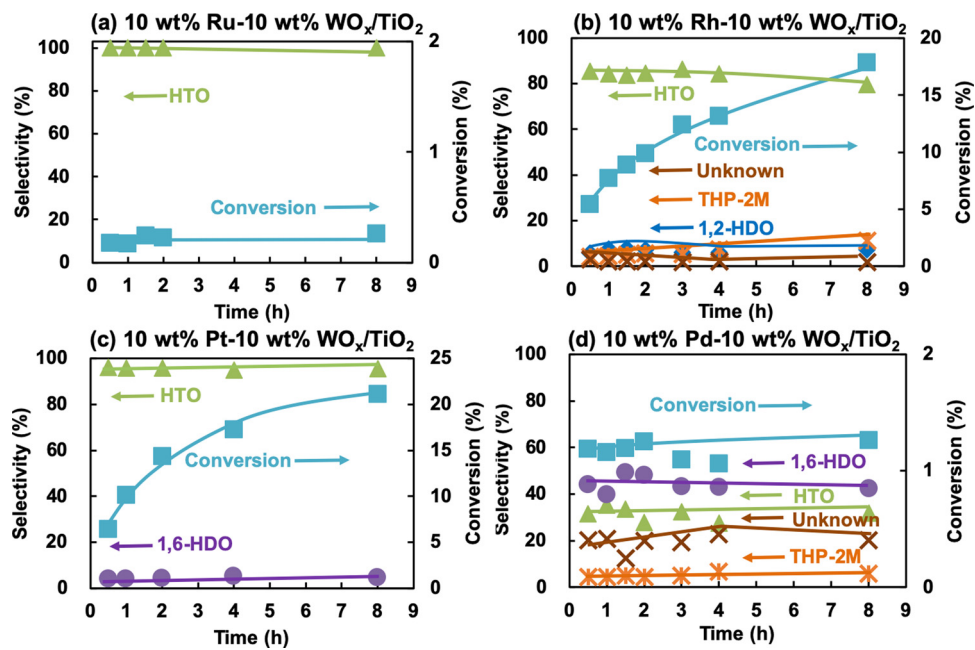


Fig. 1. THFDM (5 wt% in H_2O , 20 mL) conversion over 10 wt% metal-10 wt% WO_x/TiO_2 catalysts (0.10 g) at 160 $^{\circ}\text{C}$ under 5.5 MPa H_2 . (a) 10 wt% Ru-10 wt% WO_x/TiO_2 (b) 10 wt% Rh-10 wt% WO_x/TiO_2 (c) 10 wt% Pt-10 wt% WO_x/TiO_2 (d) 10 wt% Pd-10 wt% WO_x/TiO_2 .

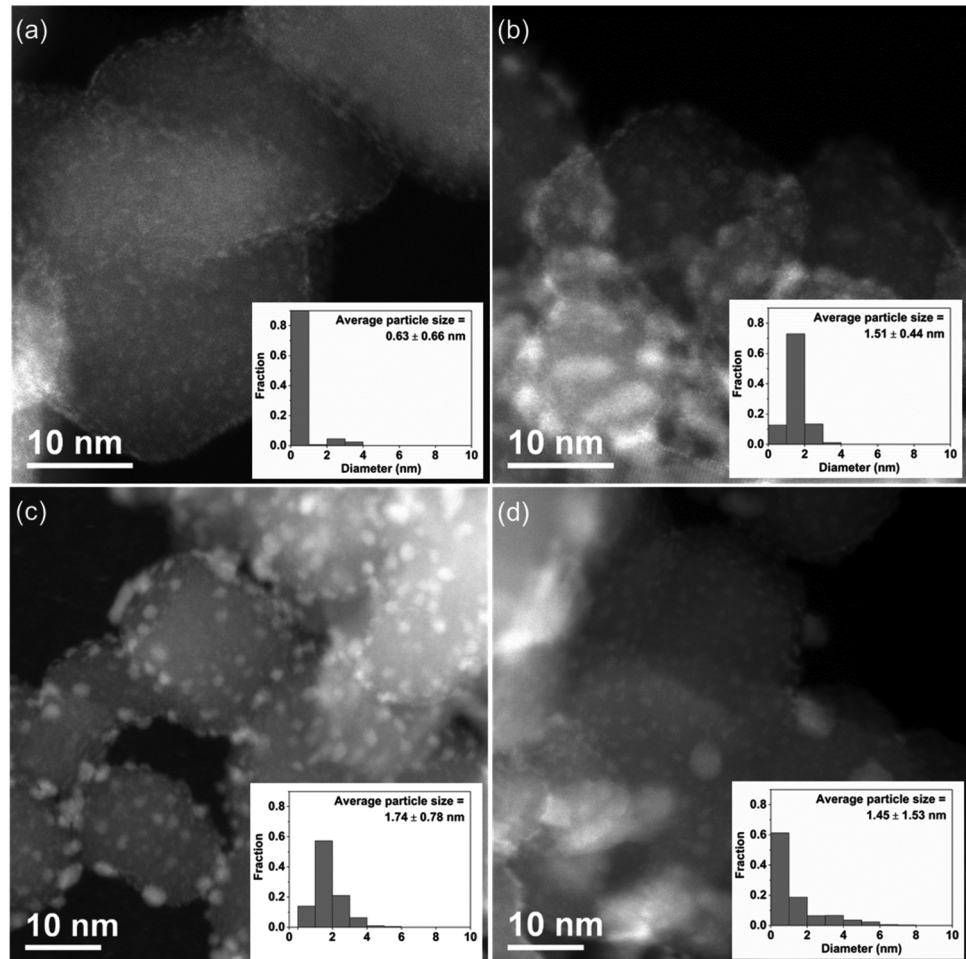
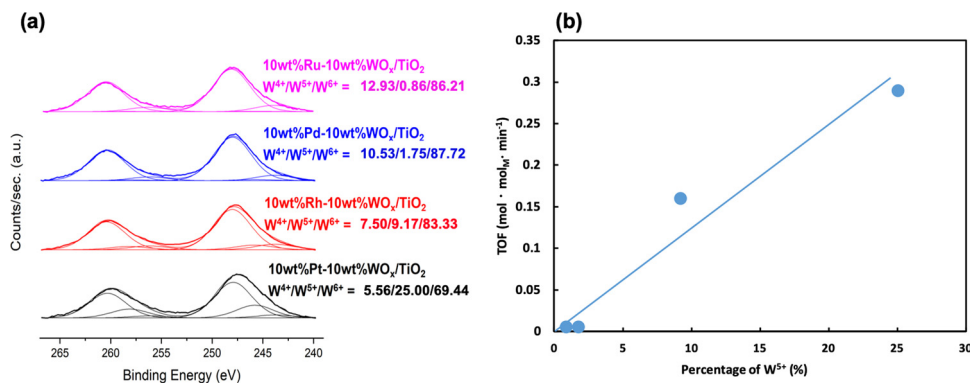


Fig. 2. STEM images of (a) 10 wt% Ru-10 wt% WO_x/TiO_2 (b) 10 wt% Rh-10 wt% WO_x/TiO_2 (c) 10 wt% Pt-10 wt% WO_x/TiO_2 (d) 10 wt% Pd-10 wt% WO_x/TiO_2 .

Table 1Properties of M-WO_x/TiO₂ (M = Pt, Pd, Rh, Ru) and Pt/TiO₂ catalysts.

Catalyst	STEM particle size (nm)	Estimated particle size from CO uptake (nm) ^a	CO uptake (μmol g ⁻¹)	TOF for THFDM conversion (mol·mol _M ⁻¹ ·min ⁻¹) ^b	TOF for THFDM conversion (mol·mol _{Surf M} ⁻¹ ·min ⁻¹) ^c
Pt-WO _x /TiO ₂	1.74 ± 0.78	6.2	85	0.29	1.60
Rh-WO _x /TiO ₂	1.51 ± 0.44	9.0	99	0.16	1.34
Pd-WO _x /TiO ₂	1.45 ± 1.53	26.1	36	0.034	0.80
Ru-WO _x /TiO ₂	0.63 ± 0.66	191.9	5	0.0059	0.85
Pt/TiO ₂	1.59 ± 0.38	2.8	177	0.044	0.11
Rh/TiO ₂	1.37 ± 0.33	5.3	201	0.082	0.40
Pd/TiO ₂	1.13 ± 0.89	24.2	38	0.003	0.065
Ru/TiO ₂	3.51 ± 1.16	183.0	32	0	0

^a The estimated particle size was calculated according to the method [55]. This assumes 100% reduction of the metal and no overcoating of the metal particle.^b TOF is normalized by the total metal atoms.^c TOF is normalized by the surface metal atoms.**Fig. 3.** (a) W 4d XPS of M-WO_x/TiO₂ catalysts after reduction under flowing H₂ at 250 °C (1 °C min⁻¹) for 2 h. (b) TOFs for THFDM conversion versus percentages of W⁵⁺ in the catalysts.

bimetallics (1.74 ± 0.78 nm for Pt and 1.51 ± 0.44 nm for Rh) of this study. This result shows that the oxophilic additive (WO_x, in this case) covers more metal sites with the Pd- and Ru-WO_x/TiO₂ (36 and 5 μmol g⁻¹) catalyst than the Pt- (85 μmol g⁻¹) and Rh-WO_x/TiO₂ catalyst (99 μmol g⁻¹) [32]. We note there is uncertainty in the particle size measurements due to the small area of the catalyst which is sampled. However, the difference between measured particle size and estimated particle size from CO chemisorption for the Ru- and Pd-WO_x/TiO₂ catalysts is much larger than what would be accounted for by error in the particle size measurements. Therefore, the low CO uptake on these catalysts is likely due to an overcoat by either WO_x or TiO₂.

Additionally, a similar phenomenon is observed on Pt-, Rh-, Pd-, and Ru/TiO₂; the STEM determined particle sizes (1.59 ± 0.38 nm, 1.37 ± 0.33 nm, 1.13 ± 0.89 nm, 3.51 ± 1.16 nm) are generally smaller than the CO-chemisorption determined ones (2.8 nm, 5.3 nm, 24.2 nm, 183.0 nm) (Entry 5–8, Table 1). On these M-TiO₂ catalysts, the TiO₂ can also overcoat the metal nanoparticles. The particle sizes determined by STEM of Pd- and Ru/TiO₂ (1.13 ± 0.89 nm, 3.51 ± 1.16 nm) are much smaller than the particle size calculated from CO chemisorption (24.2 nm, 183.0 nm) (Entry 7–8, Table 1). Since the CO does not adsorb on TiO₂, this suggests that the noble metal particles are overcoated by TiO₂. According to the literature [41–45] as the reduction temperature is increased from 200 °C to 500 °C, the quantity of adsorbed hydrogen decreases due to metal overcoating of TiO₂. The higher the reduction temperature, the higher this strong metal-support interaction. According to our STEM data and CO chemisorption, all four noble metals were coated by migrating clusters of the support oxide (TiO₂) at 250 °C in a manner similar to Strong Metal-Support Interactions (SMSI) [43,46–49]. These thin TiO_x layers form on the metal particles, physically blocking the interaction of the CO gas molecules with their surfaces. Our data also show that Pd and Ru nanoparticles have more overcoating than Pt and Rh nanoparticles.

According to literature [41,42,46,48], Pt and Rh exhibit very similar behaviors with TiO₂, while Ru tends to have more oxide overcoats than other noble metals. Additionally, it has been reported that TiO₂ overcoats on Pd are feasible at temperatures as low as 350 °C [36].

Table 1 reports the analogous data for monometallic Pt-, Rh-, Pd-, and Ru/TiO₂, which shows a similar trend. Each monometallic catalyst has a similar particle size as determined by STEM, but CO uptake is one or two orders of magnitude lower for Ru/TiO₂ (32 μmol g⁻¹) and Pd/TiO₂ (38 μmol g⁻¹) compared to Pt/TiO₂ (177 μmol g⁻¹) and Rh/TiO₂ (201 μmol g⁻¹). We also studied Ru/TiO₂ and Pd/TiO₂ with CO chemisorption with a reduction temperature of 400 °C instead of our normal 250 °C treatment. Ru/TiO₂ had a marginal increase in CO uptake with the increased reduction temperature (from 5 to 7 μmol g⁻¹). Pd/TiO₂ showed a slight decrease in CO uptake from 38 to 36 μmol g⁻¹ with the 400 °C reduction temperature. Temperature programmed reduction and XPS experiments also suggest that the low CO uptake for these catalysts is not due to a difficult-to-reduce mixed oxide phase (Figs. S5 and S6) [50–54]. These data indicate that the Ru and Pd catalysts show low CO uptakes and activities due to the reduced metal being overcoated by TiO₂ in M-TiO₂ or WO_x/TiO₂ in M-WO_x/TiO₂.

3.2. Characterization of M-WO_x/TiO₂ by XPS

Fig. 3a shows the W 4d XPS data for each M-WO_x/TiO₂ catalyst after being reduced under H₂ flow at 250 °C for 2 h. As we have shown in our previous paper, Pt-WO_x/TiO₂ displays mainly W⁵⁺ and W⁶⁺ under these reduction conditions [12]. Furthermore, we concluded that the creation of this W⁵⁺ site during reduction corresponded with the production of a W-OH site, which was active for C-O bond activation in THFDM [12]. There is another signal centered at 283.8 eV in each spectrum which is assigned to the 4d_{5/2} electron of W⁴⁺ [56]. Fig. 3a shows that Pt-WO_x/TiO₂ has the highest percentage of W⁵⁺ compared

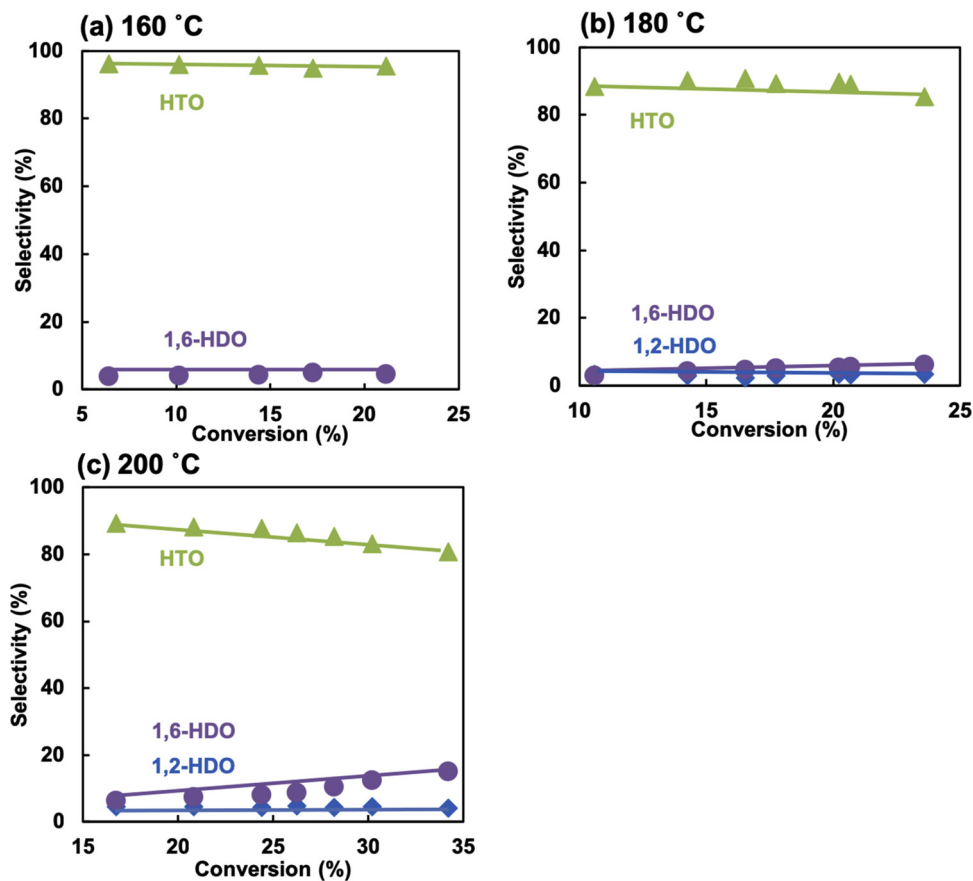


Fig. 4. THFDM (5 wt% in H₂O, 20 mL) conversion and product selectivity over 10 wt% Pt-10 wt% WO_x/TiO₂ (0.10 g) catalysts under 5.5 MPa H₂ at (a) 160 °C (b) 180 °C (c) 200 °C.

to the other catalysts. Fig. 3b shows that there is a correlation for these four catalysts between the TOF for THFDM conversion and the percentage of W⁵⁺ in the catalysts. The TOF for THFDM conversion increases with increasing W⁵⁺ in catalysts (Fig. 3b). Besides the positive correlation between percentage of W⁵⁺ and reactivity, it is also noted that there is a negative correlation between the percentage of W⁴⁺ and the catalytic activity. It has been previously reported that, for Pt/WO_x catalysts, H atoms become protons and electrons when in contact with the WO₃. The electrons reduce W⁶⁺ cations to W⁵⁺ cations and move through the WO₃ lattice by W⁵⁺ – W⁶⁺ exchange. Therefore, W⁵⁺ – W⁶⁺ exchange is important for the high activity of catalysts [57,58]. It has also been reported that the catalytic redox cycle of W⁵⁺ – W⁵⁺ produces the active site in Pt-WO_x/TiO₂ for C–O hydrogenolysis of glycerol, and the over-reduction of W⁵⁺ to the inactive W⁴⁺ species decreases activity [33].

3.3. Temperature effects of THFDM conversion over Pt-WO_x/TiO₂

Fig. 4 shows the effect of reaction temperature on THFDM conversion for the Pt-WO_x/TiO₂ catalyst. The TOF for THFDM conversion increases from 0.29 mol·mol_{Pt}⁻¹·min⁻¹ at 160 °C to 0.54 mol·mol_{Pt}⁻¹·min⁻¹ at 180 °C to 0.87 mol·mol_{Pt}⁻¹·min⁻¹ at 200 °C. Higher temperatures also lead to higher selectivity to secondary products (1,6-HDO and 1,2-HDO). However, Fig. 4 shows that HTO hydrogenolysis over Pt-WO_x/TiO₂ favors 1,6-HDO, our desired final product, over the less-desirable 1,2-HDO. 1,6-HDO selectivity increases from 4.5% at 160 °C to 6% at 180 °C to 15% at 200 °C, while 1,2-HDO selectivity increases from 0% at 160 °C to 3.3% at 180 °C to 4% at 200 °C (Fig. 4). The apparent activation energy for THFDM conversion is calculated to be 47 kJ·mol⁻¹ (Fig. 5).

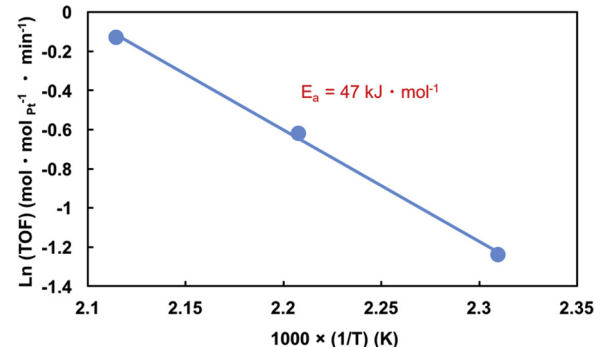


Fig. 5. Arrhenius plot for THFDM conversion. Reaction conditions: THFDM (5 wt% in H₂O, 20 mL), 0.10 g 10 wt% Pt-10 wt% WO_x/TiO₂ under 5.5 MPa H₂.

3.4. H₂ pressure effect of THFDM hydrogenolysis over Pt-WO_x/TiO₂

The effect of reaction pressure on THFDM conversion is shown in Fig. 6. Figs. 6a and b show that THP-2 M selectivities of up to 30% are achieved at low reaction pressures and low conversions. No THP-2 M is observed at pressures of 3.4 and 5.5 MPa, with HTO being the primary product (Figs. 6a and b). As shown in Fig. S2, the HTO selectivity increases gradually from 70% at 1.0 MPa to 95% at 5.5 MPa H₂, while the THP-2 M selectivity decreases from 16% at 1.0 MPa to 0% at 3.4 MPa H₂. This result supports Scheme 1 which shows that there are two pathways for conversion of THFDM into HTO. The first pathway is through THP-2 M while the second pathway involves direct conversion of THFDM into HTO. Both of these pathways first involve a ring opening of the THFDM by a hydrogenolysis step which likely involves an oxocarbenium ion [16]. HTO is likely formed from hydrogenation of

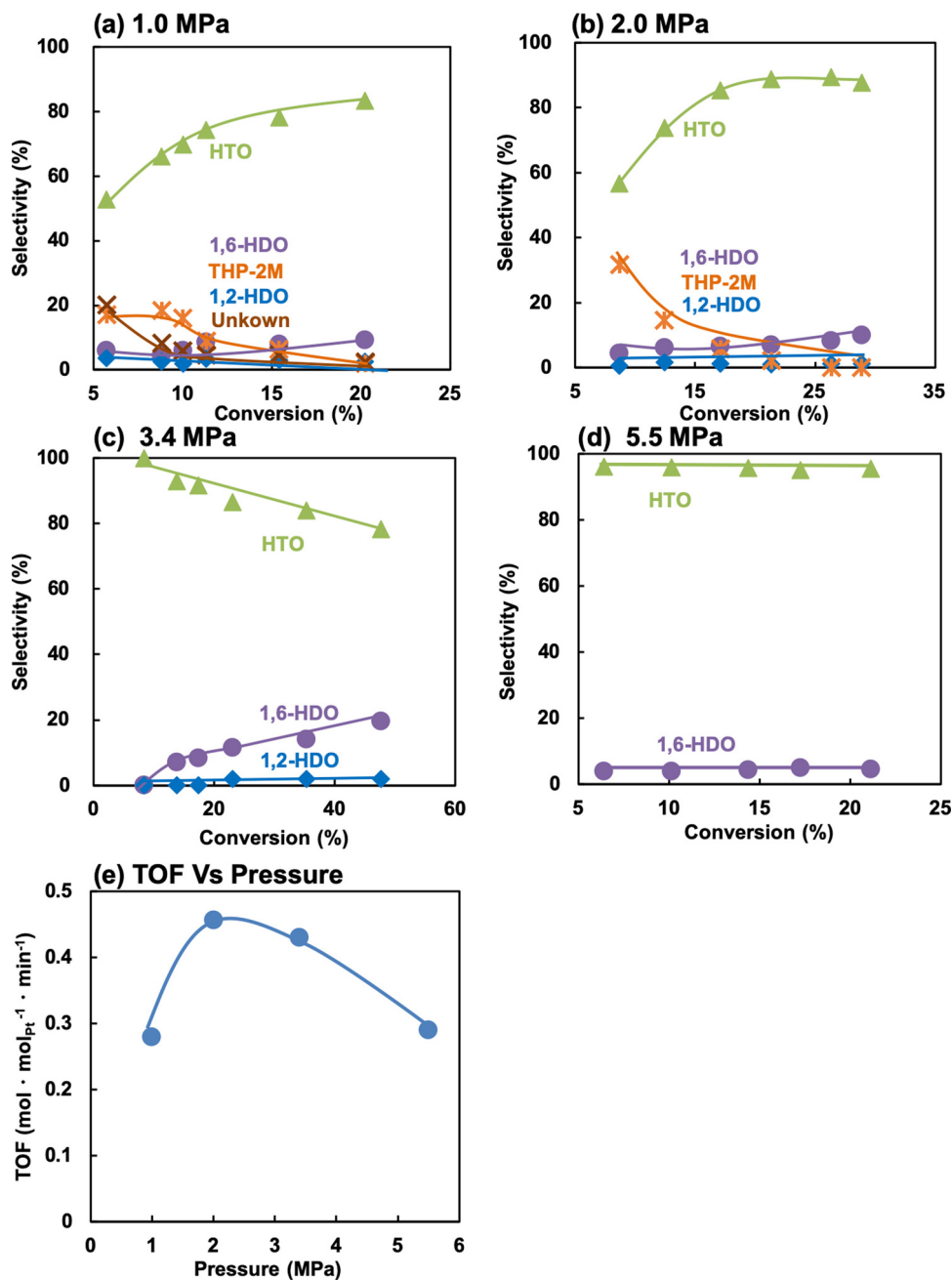


Fig. 6. THFDM (5 wt% in H_2O , 20 mL) conversion and product selectivities over 10 wt% Pt-10 wt% WO_x/TiO_2 (0.10 g) catalysts at 160 °C under (a) 1.0 MPa H_2 (b) 2.0 MPa H_2 (c) 3.4 MPa H_2 (d) 5.5 MPa H_2 (e) TOFs for THFDM conversion versus reaction pressure.

this oxocarbenium ion, while THP-2 M is likely formed by a ring closing dehydration of the oxocarbenium ion followed by hydrogenation (see proposed reaction pathway in **Scheme S2**). **Fig. 6e** shows that the TOF for THFDM conversion passes through a maximum of $0.45 \text{ mol}_{\text{Pt}}^{-1} \cdot \text{min}^{-1}$ at 2.0 MPa, then gradually decreases to $0.29 \text{ mol}_{\text{Pt}}^{-1} \cdot \text{min}^{-1}$ at 5.5 MPa.

Fig. 7 shows the XPS of the Pt/ WO_x/TiO_2 catalyst as a function of hydrogen pressure. **Fig. 7a** shows the Pt 4f region of Pt- WO_x/TiO_2 after reduction at various H_2 pressures at 250 °C. This data indicates that H_2 pressure does not change the oxidation state of Pt. **Fig. 7b** shows the W 4d region of each of these catalysts. We can see that the H_2 pressure used during reduction has a strong effect on the W oxidation state. Specifically, we see that the amount of W^{4+} and W^{5+} relative to W^{6+} increases with increasing reduction pressure. This behavior agrees with the studies of Wang *et al.*, in which they also observed maximum

activity at an intermediate H_2 pressure for glycerol hydrogenolysis with Pt/ WO_x [33]. The lower activity at higher H_2 pressure was partly attributed to the further reduction of W^{5+} to W^{4+} [33]. According to **Fig. 7b**, the percentage of W^{4+} increases with increasing H_2 pressure, while the percentage of W^{5+} remains almost constant. As discussed in Section 3.2, the higher percentage of W^{4+} could be a factor which can lower the TOF of THFDM conversion. The appearance of a maximum TOF with increasing H_2 pressure demonstrates that hydrogen can inhibit the reaction at higher hydrogen pressures indicating that high hydrogen coverages can occur on this catalyst. As shown in **Fig. S3**, the reaction is first order with respect to THFDM at 5.5 MPa H_2 , indicating that THFDM does not inhibit the reaction. Thus, hydrogen can have two roles in influencing the catalyst: 1) strongly adsorbing and inhibiting the activity [59–62] and 2) reducing the W to a less active form [33].

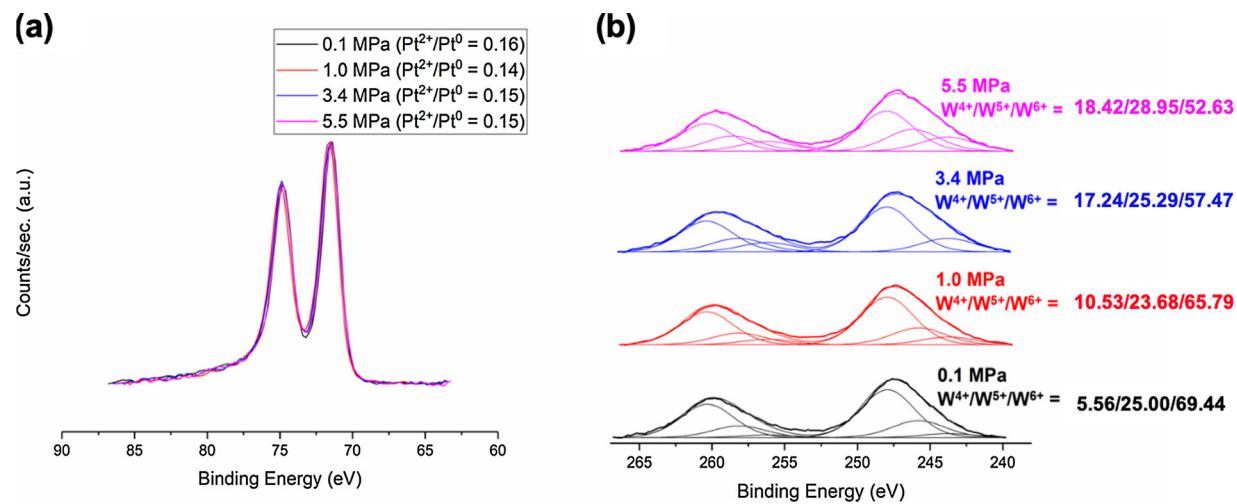


Fig. 7. XPS of (a) Pt 4f and (b) W 4d regions after reduction treatments at various pressures.

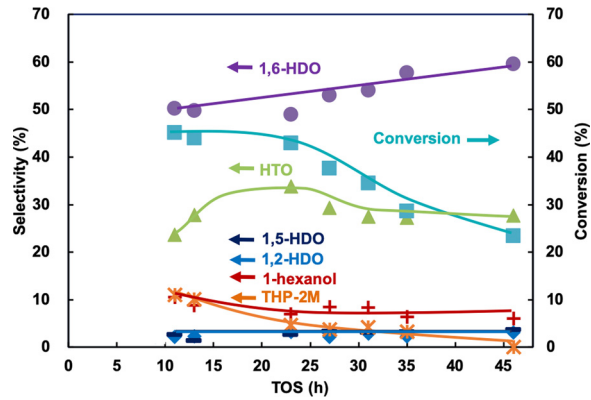


Fig. 8. THFDM conversion in a continuous flow reactor. Reaction conditions: 1% aq. THFDM, 10 wt%Pt- 10 wt% WO_x/TiO_2 , WHSV = 1.3 h^{-1} , 160 $^{\circ}\text{C}$, 3.4 MPa H_2 .

3.5. THFDM conversion over Pt- WO_x/TiO_2 in a continuous flow reactor

The Pt- WO_x/TiO_2 catalyst was then studied in a fixed-bed reactor for conversion of THFDM to 1,6-HDO shown in Fig. 8. 1,6-HDO is the main product, with selectivity increasing throughout the reaction in the range of 50–60%. The HTO selectivity increases at low time-on-stream (TOS) and then stabilizes just below 30%. THP-2 M is also formed with 15% selectivity at low time-on-stream. Combining selectivities to 1,6-HDO, HTO, and THP-2 M, we see that the total selectivity to 1,6-HDO and its precursors exceeds 80% at each point in the reaction. Less desirable products such as 1-hexanol, 1,5-hexanediol (1,5-HDO), and 1,2-HDO, are also formed with < 20% combined selectivity due to the over-hydrogenolysis of 1,6-HDO and non-selective hydrogenolysis of HTO. The conversion decreases from 45% to 23% over the course of 46 h on stream.

Tungsten was observed in the effluent liquid product. W concentrations leached in the effluent have been determined by ICP. Based on these concentrations, the remaining W in the reactor is calculated after accounting for what was detected in the effluent. The tungsten leaching rate, defined as the percentage of the initial tungsten on the catalyst that is removed each hour, as a function of TOS is shown in Fig. 9. The tungsten leaching rate decreased from 0.49% $\text{W}\cdot\text{h}^{-1}$ at 11 h TOS to 0.22% $\text{W}\cdot\text{h}^{-1}$ at 57 h TOS, while the remaining W in the catalysts decreased from 95.3% W at 11 h TOS to 79.0% at 57 h TOS. The leaching of Pt is negligible (< 0.002%). It is likely that tungsten leaching is leading to the deactivation of Pt- WO_x/TiO_2 , which is shown in Fig. 8 by the decrease in conversion with increasing TOS.

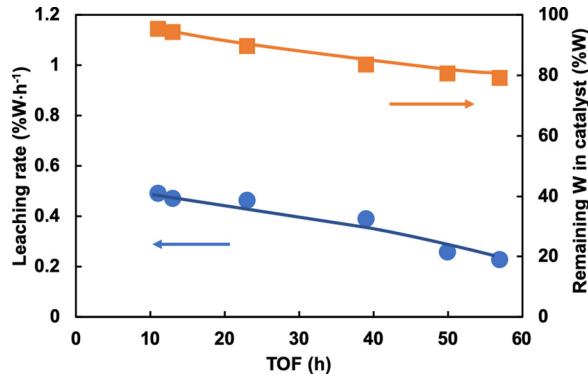


Fig. 9. Tungsten leaching rate of 10 wt% Pt-10 wt% WO_x/TiO_2 in the continuous flow reactor.

3.6. THFDM hydrogenolysis with Pt/TiO₂ with homogeneous W salts

Djakovitch and Pinel *et al.* reported that the addition of W acid/salts to Rh/C greatly accelerates the glycerol conversion and selectivity to 1,3-propanediol in the glycerol hydrogenolysis in the aqueous phase under 8 MPa H_2 at 180 $^{\circ}\text{C}$ [63]. To further investigate the effect of W leaching in our catalytic system and identify the extent to which the leached W contributes to the catalytic activity, we investigated the addition of homogeneous W salts to the THFDM solution. The TOFs of THFDM conversion and product selectivities over pure Pt/TiO₂ and Pt/TiO₂ with 0.029 mmol L⁻¹ ammonium metatungstate (AMT) are nearly identical (Fig. 10), which indicates that the small amount of AMT (equivalent to 12% of the W in 0.10 g of 10 wt% WO_x/TiO_2 , which represents a much higher homogeneous W concentration than that of the leached W in 8 h in the actual batch reaction (< 4%)) has no influence on the Pt/TiO₂ activity (Figs. 10a and b). The TOF of THFDM conversion increases from 0.042 mol·mol_{Pt}⁻¹·min⁻¹ with 0.029 mmol L⁻¹ AMT to a maximum of 0.27 mol·mol_{Pt}⁻¹·min⁻¹ with 0.14 mmol L⁻¹ AMT and then decreases to 0.14 mol·mol_{Pt}⁻¹·min⁻¹ with 0.40 mmol L⁻¹ AMT (Fig. 11). Therefore, THFDM can be efficiently converted to HTO in the presence of Pt/TiO₂ and higher than 0.14 mmol L⁻¹ of homogeneous W salts. The W concentration in the presence of 0.029 mmol L⁻¹ AMT is at least three times higher than what is present during leaching of Pt- WO_x/TiO_2 at conditions reported in Figs. 8 and 9. Therefore, we conclude that the W leached from the Pt- WO_x/TiO_2 catalyst does not contribute to the overall THFDM conversion rate.

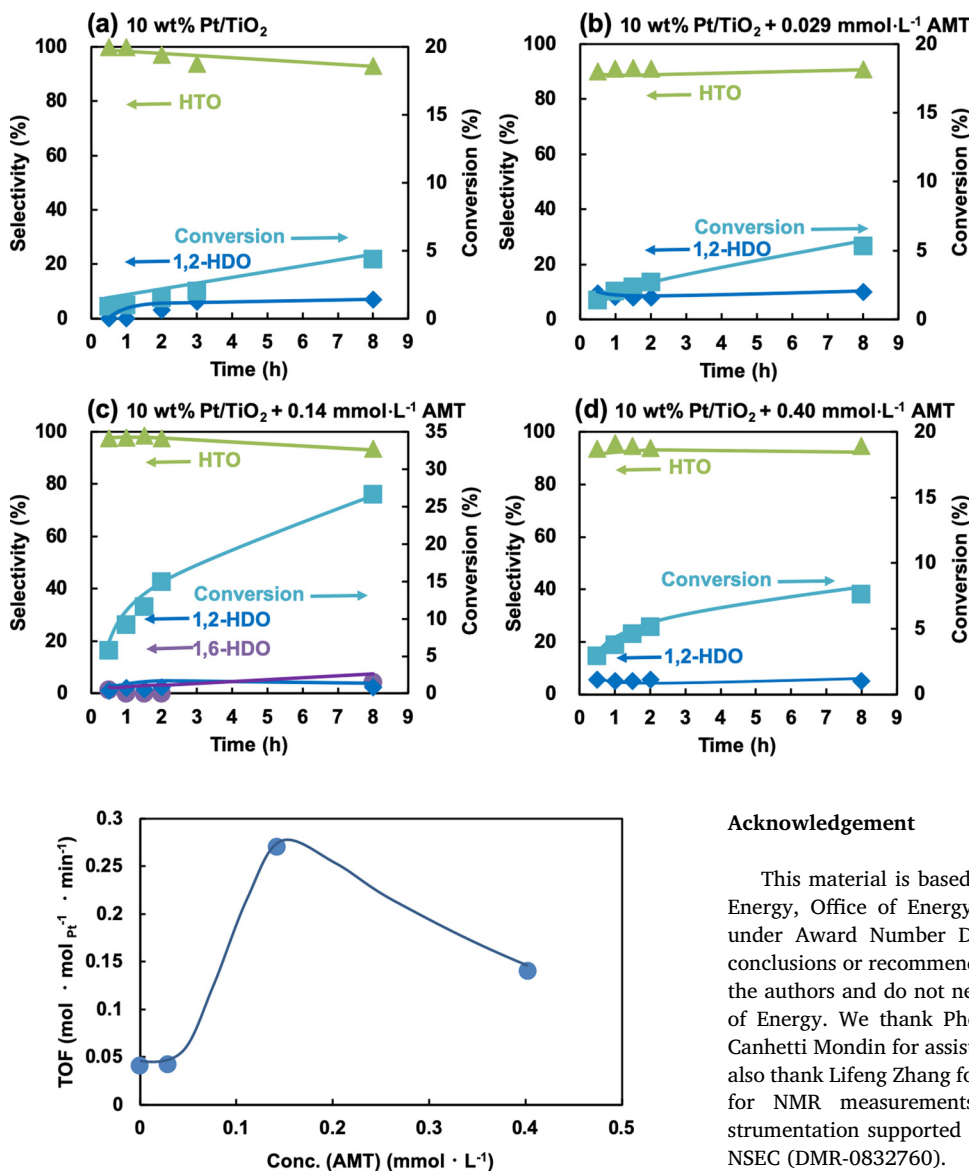


Fig. 11. THFDM (5 wt% in H_2O , 20 mL) conversion rate over 10 wt% Pt/TiO_2 (0.10 g) catalysts and various concentrations of AMT salts at 160 $^{\circ}\text{C}$ under 5.5 MPa H_2 .

4. Conclusions

$\text{Pt-WO}_x/\text{TiO}_2$ and $\text{Rh-WO}_x/\text{TiO}_2$ have two orders-of-magnitude higher catalytic activity (per metal site) than Ru- and Pd- WO_x/TiO_2 for THFDM hydrogenolysis. This enhanced activity is due to two effects 1) WO_x/TiO_2 overcoats Ru and Pd more than Pt and Rh, and 2) Pt and Rh are able to more effectively reduce of W^{6+} to the active W^{5+} . $\text{Pt-WO}_x/\text{TiO}_2$ has almost twice the activity (per metal site) of $\text{Rh-WO}_x/\text{TiO}_2$ for this reaction, even though $\text{Rh-WO}_x/\text{TiO}_2$ has slightly higher CO uptake. The THFDM reaction rate passes through a maximum of $0.45 \text{ mol} \cdot \text{mol}_{\text{Pt}}^{-1} \cdot \text{min}^{-1}$ with hydrogen pressure indicating that at high pressure the surface is highly covered with hydrogen. Increasing the hydrogen pressure also reduces the W oxidation state in the catalyst. In the range of 160–200 $^{\circ}\text{C}$, we show that combined selectivity to 1,6-HDO and HTO remains above 90%. The apparent activation energy for THFDM conversion of $47 \text{ kJ} \cdot \text{mol}^{-1}$. The conversion decreased from 45% at 11 h to 23% at 46 h over $\text{Pt-WO}_x/\text{TiO}_2$ under continuous-flow conditions, while selectivities to 1,6-HDO and its precursors remain high. Catalyst deactivation is likely due to tungsten leaching.

Fig. 10. THFDM (5 wt% in H_2O , 20 mL) conversion over 10 wt% Pt/TiO_2 (0.10 g) catalysts and AMT salts at 160 $^{\circ}\text{C}$ under 5.5 MPa H_2 (a) without AMT (b) with $0.029 \text{ mmol L}^{-1}$ AMT (equivalent to 12% of the W of 0.10 g 10 wt% WO_x/TiO_2) (c) with 0.14 mmol L^{-1} AMT (equivalent to 62% of the W of 0.10 g 10 wt% WO_x/TiO_2) (d) with 0.40 mmol L^{-1} AMT (equivalent to 178% of the W of 0.10 g 10 wt% WO_x/TiO_2).

Acknowledgement

This material is based upon work supported by the Department of Energy, Office of Energy Efficiency and Renewable Energy (EERE), under Award Number DE-EE0006878. Any opinions, findings, and conclusions or recommendations expressed in this material are those of the authors and do not necessarily reflect the views of the Department of Energy. We thank Phoebe Wagner, Xiaoli Chen, Giulia Kitayama Canhetti Mondin for assistance with THFDM and catalyst synthesis. We also thank Lifeng Zhang for XPS measurements and Daniel J McClelland for NMR measurements. The authors acknowledge use of instrumentation supported by UW MRSEC (DMR-1121288) and the UW NSEC (DMR-0832760).

Appendix A. Supplementary data

Supplementary material related to this article can be found, in the online version, at doi:<https://doi.org/10.1016/j.apcatb.2019.117945>.

References

- [1] G.W. Huber, S. Iborra, A. Corma, Synthesis of transportation fuels from biomass: chemistry, catalysts, and engineering, *Chem. Rev.* 106 (2006) 4044–4098, <https://doi.org/10.1021/cr068360d>.
- [2] T. Werpy, G. Petersen, *Top Value Added Chemicals From Biomass: Volume I- Results of Screening for Potential Candidates From Sugars and Synthesis Gas*, Golden, CO, 2004.
- [3] G. Cinti, R.A. Van Santen, *Catalysis for Renewables: From Feedstock to Energy Production*, (2007), <https://doi.org/10.1002/9783527621118>.
- [4] M. De bruyn, J. Fan, V.L. Budarin, D.J. Macquarrie, L.D. Gomez, R. Simister, T.J. Farmer, W.D. Raverty, S.J. McQueen-Mason, J.H. Clark, A new perspective in bio-refining: levoglucosanone and cleaner lignin from waste biorefinery hydrolysis lignin by selective conversion of residual saccharides, *Energy Environ. Sci.* 9 (2016) 2571–2574, <https://doi.org/10.1039/C6EE01352J>.
- [5] F. Cao, T.J. Schwartz, D.J. McClelland, S.H. Krishna, J.A. Dumesic, G.W. Huber, Dehydration of cellulose to levoglucosanone using polar aprotic solvents, *Energy Environ. Sci.* 8 (2015) 1808–1815, <https://doi.org/10.1039/C5EE00353A>.
- [6] MarketsandMarkets, *1,6-Hexanediol Market by Application (Polyurethanes, Coatings, Acrylates, Adhesives, Unsaturated Polyester Resins, Plasticizers, and Others) - Trends and Forecasts to 2019*, (2014).
- [7] P. Werle, M. Morawietz, S. Lundmark, K. Sørensen, E. Karvinen, J. Lehtonen, Alcohols, polyhydric, Ullmann's Encycl. Ind. Chem. (2008) 263–281, <https://doi.org/10.1002/14356007.a01>.

- [8] D.E. Mears, A.D. Eastman, Kirk-Othmer Encyclopedia of Chemical Technology, (2014).
- [9] W.D. Fisher, J.F. VanPeppen, Kirk-Othmer Encyclopedia of Chemical Technology, (2000).
- [10] J.P. Oppenheim, G.L. Dickerson, Kirk-Othmer Encyclopedia of Chemical Technology, (2014).
- [11] K.G. Baur, R. Fischer, R. Pinkos, F. Stein, H. Rust, B. Breitscheidel, Process for preparing 1,6 hexanediol with a level of purity over 99%, US Patent US6008418A, 1999.
- [12] J. He, S.P. Burt, M. Ball, D. Zhao, I. Hermans, J.A. Dumesic, G.W. Huber, Synthesis of 1,6-Hexanediol from cellulose derived tetrahydrofuran-dimethanol with Pt-WO_x/TiO₂Catalysts, *ACS Catal.* 8 (2018) 1427–1439, <https://doi.org/10.1021/acs.catal.7b03593>.
- [13] M. Faber, *Process for Producing Adipic Acid From Biomass*, 4,400,468 (1983).
- [14] T. Buntara, S. Noel, P.H. Phua, I. Melián-Cabrera, J.G. De Vries, H.J. Heeres, Caprolactam from renewable resources: catalytic conversion of 5-hydroxymethylfurfural into caprolactone, *Angew. Chemie - Int. Ed.* 50 (2011) 7083–7087, <https://doi.org/10.1002/anie.201102156>.
- [15] T. Buntara, I. Melián-Cabrera, Q. Tan, J.L.G. Fierro, M. Neurock, J.G. De Vries, H.J. Heeres, Catalyst studies on the ring opening of tetrahydrofuran-dimethanol to 1,2,6-hexanetriol, *Catal. Today* 210 (2013) 106–116, <https://doi.org/10.1016/j.cattod.2013.04.012>.
- [16] M. Chia, Y.J. Pagán-Torres, D. Hibbitts, Q. Tan, H.N. Pham, A.K. Datye, M. Neurock, R.J. Davis, J.A. Dumesic, Selective hydrogenolysis of polyols and cyclic ethers over bifunctional surface sites on rhodium-rhenium catalysts, *J. Am. Chem. Soc.* 133 (2011) 12675–12689, <https://doi.org/10.1021/ja2038358>.
- [17] K. Chen, S. Koso, T. Kubota, Y. Nakagawa, K. Tomishige, Chemoselective Hydrogenolysis of Tetrahydropyran-2-methanol to 1,6-Hexanediol over rhenium-modified carbon-supported rhodium catalysts, *ChemCatChem.* 2 (2010) 547–555, <https://doi.org/10.1002/cctc.201000018>.
- [18] S.P. Burt, K.J. Barnett, D.J. McClelland, P. Wolf, J.A. Dumesic, G.W. Huber, I. Hermans, Production of 1,6-hexanediol from tetrahydropyran-2-methanol by dehydration-hydration and hydrogenation, *Green Chem.* 19 (2017) 1390–1398, <https://doi.org/10.1039/c6gc03606f>.
- [19] A.M. Allgeier, W.I.N. De Silva, E. Korovessi, C.A. Menning, J.C. Ritter, S.K. Sengupta, C.S. Stauffer, *Process for Preparing 1,6-hexanediol*, (2014).
- [20] V. Sokolovskii, M. Lavrenko, A. Hagemeyer, E. Dias, J.A. Shoemaker, V.J. Murphy, *Process for Production of Hexanetriol From 5-Hydroxymethylfurfural*, US 9,586,920 B2 (2017).
- [21] W. Karim, C. Spreafield, A. Kleibert, J. Gobrecht, J. VandeVondele, Y. Ekinci, J.A. van Bokhoven, Catalyst support effects on hydrogen spillover, *Nature* 541 (2017) 68–71, <https://doi.org/10.1038/nature20782>.
- [22] P. Frediani, U. Matteoli, M. Bianchi, F. Piacenti, G. Menchi, Cluster ruthenium hydrogenation catalysts, *J. Organomet. Chem.* 150 (1978) 273–278, [https://doi.org/10.1016/S0022-328X\(00\)84730-0](https://doi.org/10.1016/S0022-328X(00)84730-0).
- [23] J.M. Tour, J.P. Cooper, S.L. Pendalwar, Highly selective heterogeneous palladium-catalyzed hydrogenations using triethoxysilane and water, *J. Org. Chem.* 55 (1990) 3452–3453.
- [24] W.S. Knowles, *Asymmetric hydrogenations*, *Angew. Chemie - Int. Ed.* 41 (2002) 1998–2007.
- [25] D.M. Alonso, S. Hakim, S. Zhou, W. Won, O. Hosseinaei, J. Tao, V. Garcia-Negrón, A.H. Motagamwala, M.A. Mellmer, K. Huang, C.J. Houtman, N. Labbé, D.P. Harper, C. Maravelias, T. Runge, J.A. Dumesic, Increasing the revenue from lignocellulosic biomass: maximizing feedstock utilization, *ScienceAdvances* (2017), <https://doi.org/10.1126/sciadv.1603301>.
- [26] J. He, M. Liu, K. Huang, T.W. Walker, C.T. Maravelias, J.A. Dumesic, G.W. Huber, Production of levoglucosanone and 5-hydroxymethylfurfural from cellulose in polar aprotic solvent–water mixtures, *Green Chem.* 19 (2017) 3642–3653, <https://doi.org/10.1039/C7GC01688C>.
- [27] S.H. Krishna, D.J. McClelland, Q.A. Rashke, J.A. Dumesic, G.W. Huber, Hydrogenation of levoglucosanone to renewable chemicals, *Green Chem.* 19 (2017) 1278–1285, <https://doi.org/10.1039/C6GC03028A>.
- [28] J. He, K. Huang, K.J. Barnett, S. Krishna, D.M. Alonso, Z.J. Brentzel, S.P. Burt, T. Walker, W.F. Banholzer, C.T. Maravelias, I. Hermans, J.A. Dumesic, G.W. Huber, New catalytic strategies for α,ω -diols production from lignocellulosic biomass, *Faraday Discuss.* 202 (2017) 247–267, <https://doi.org/10.1039/C7FD00036G>.
- [29] S.H. Krishna, K. Huang, K.J. Barnett, J. He, C.T. Maravelias, J.A. Dumesic, G.W. Huber, M. De bruyn, B.M. Weckhuysen, Oxygenated commodity chemicals from chemo-catalytic conversion of biomass derived heterocycles, *AIChE J.* 64 (2018) 1910–1922, <https://doi.org/10.1002/aic.16172>.
- [30] Y. Amada, Y. Shimini, S. Koso, T. Kubota, Y. Nakagawa, K. Tomishige, Reaction mechanism of the glycerol hydrogenolysis to 1,3-propanediol over Ir-ReO_x/SiO₂ catalyst, *Appl. Catal. B Environ.* 105 (2011) 117–127, <https://doi.org/10.1016/j.apcatb.2011.04.001>.
- [31] K. Tomishige, Y. Nakagawa, M. Tamura, Metal catalysts directly modified with metal oxide, *Green Chem.* 19 (2017) 2876–2924, <https://doi.org/10.1039/c7gc01763a>.
- [32] P.U. Karanjkar, S.P. Burt, X. Chen, K.J. Barnett, M.R. Ball, M.D. Kumbhalkar, X. Wang, J.B. Miller, I. Hermans, J.A. Dumesic, G.W. Huber, Effect of carbon supports on Rh/Re bifunctional catalysts for selective hydrogenolysis of tetrahydropyran-2-methanol, *Catal. Sci. Technol.* 6 (2016) 7841–7851, <https://doi.org/10.1039/c6cy01763k>.
- [33] J. Wang, X. Zhao, N. Lei, L. Li, L. Zhang, S. Xu, S. Miao, X. Pan, A. Wang, T. Zhang, Hydrogenolysis of glycerol to 1,3-propanediol under low hydrogen pressure over WO_x-Supported Single/Pseudo-Single atom Pt catalyst, *ChemSusChem.* 9 (2016) 784–790, <https://doi.org/10.1002/cssc.201501506>.
- [34] S. García-Fernández, I. Gandarias, J. Requies, M.B. Güemez, S. Bennici, A. Auroux, P.L. Arias, New approaches to the Pt/WO_x/Al2O3 catalytic system behavior for the selective glycerol hydrogenolysis to 1,3-propanediol, *J. Catal.* 323 (2015) 65–75, <https://doi.org/10.1016/j.jcat.2014.12.028>.
- [35] S. Zhu, X. Gao, Y. Zhu, J. Cui, H. Zheng, Y. Li, SiO₂ promoted Pt/WO_x/ZrO₂ catalysts for the selective hydrogenolysis of glycerol to 1,3-propanediol, *Appl. Catal. B Environ.* 158–159 (2014) 391–399, <https://doi.org/10.1016/j.apcatb.2014.04.049>.
- [36] J. Sá, J. Bernardi, J.A. Anderson, Imaging of low temperature induced SMSI on Pt/TiO₂ catalysts, *Catal. Letters* 114 (2007) 91–95, <https://doi.org/10.1007/s10562-007-9049-1>.
- [37] X. Shen, L.-J. Garces, Y. Ding, K. Laubernds, R.P. Zerger, M. Aindow, E.J. Neth, S.L. Suib, Behavior of H₂ chemisorption on Ru/TiO₂ surface and its application in evaluation of Ru particle sizes compared with TEM and XRD analyses, *Appl. Catal. A Gen.* 335 (2008) 187–195, <https://doi.org/10.1016/j.apcata.2007.11.017>.
- [38] Y.V. Larichev, O.V. Netskina, O.V. Komova, V.I. Simagina, Comparative XPS study of Rh/Al2O3 and Rh/TiO₂ as catalysts for NaBH₄ hydrolysis, *Int. J. Hydrogen Energy* 35 (2010) 6501–6507, <https://doi.org/10.1016/j.ijhydene.2010.04.048>.
- [39] M. Englisch, A. Jentsch, J.A. Lercher, Structure sensitivity of the hydrogenation of Crotonaldehyde over Pt/SiO₂and Pt/TiO₂, *J. Catal.* 166 (1997) 25–35, <https://doi.org/10.1006/jcat.1997.1494>.
- [40] L. Jiao, J.R. Regalbuto, The synthesis of highly dispersed noble and base metals on silica via strong electrostatic adsorption: I. Amorphous silica, *J. Catal.* 260 (2008) 329–341, <https://doi.org/10.1016/j.jcat.2008.09.022>.
- [41] S.J. Tauster, S.C. Fung, R.L. Garten, Strong metal-support interactions. Group 8 noble metals supported on TiO₂, *J. Am. Chem. Soc.* 100 (1978) 170–175, <https://doi.org/10.1021/ja00469a029>.
- [42] G.L. Haller, D.E. Resasco, Metal-support interaction group VIII metals and reducible oxides, *Adv. Catal.* 36 (1989) 173–235, [https://doi.org/10.1016/S0360-0564\(08\)60018-8](https://doi.org/10.1016/S0360-0564(08)60018-8).
- [43] J.D. Bracey, R. Burch, Enhanced activity of Pd TiO₂ catalysts for the CO H₂ reaction in the absence of strong metal-support interactions (SMSI), *J. Catal.* 86 (1984) 384–391, [https://doi.org/10.1016/0021-9517\(84\)90383-X](https://doi.org/10.1016/0021-9517(84)90383-X).
- [44] M.S. Spencer, Models of strong metal-support interaction (SMSI) in Pt on TiO₂ catalysts, *J. Catal.* 93 (1985) 216–223, [https://doi.org/10.1016/0021-9517\(85\)90169-1](https://doi.org/10.1016/0021-9517(85)90169-1).
- [45] S.J. Tauster, Strong metal support interaction, *Acc. Chem. Res.* 20 (1987) 389–394, <https://doi.org/10.1016/B978-0-444-81468-5.50015-7>.
- [46] S. Zhang, P.N. Plessow, J.J. Willis, S. Dai, M. Xu, G.W. Graham, M. Cargnello, F. Abild-Pedersen, X. Pan, Dynamical observation and detailed description of catalysts under strong metal-support interaction, *Nano Lett.* 16 (2016) 4528–4534, <https://doi.org/10.1021/acs.nanolett.6b01769>.
- [47] A. David Logan, E.J. Braunschweig, A.K. Datye, D.J. Smith, Direct observation of the surfaces of small metal crystallites: rhodium supported on TiO₂, *Langmuir* 4 (1988) 827–830, <https://doi.org/10.1021/la00082a009>.
- [48] A.K. Datye, D.S. Kalakad, M.H. Yao, D.J. Smith, Comparison of Metal-Support Interactions in Pt-TiO₂ and Pt-CeO₂, *J. Catal.* 1995, *J. Catal.* 155 (1995) 148–153, <https://doi.org/10.1016/j.cat.1995.1196>.
- [49] J. Liu, Advanced Electron microscopy characterization of nanostructured heterogeneous catalysts, *Microsc. Microanal.* 10 (2004) 55–76, <https://doi.org/10.1017/S1431927604040310>.
- [50] J. Goralski, V.S. Federyeva, R.F. Vitkovskaya, M. Szinkowska, Study of properties of Al2O3 and TiO₂ supported palladium catalysts in reactions of tetrachloromethane hydrogenation, *Russ. J. Appl. Chem.* 85 (2012) 598–603, <https://doi.org/10.1134/S1070427120404118>.
- [51] H. Zhu, Z. Qin, W. Shan, W. Shen, J. Wang, Pd/CeO₂-TiO₂ catalyst for CO oxidation at low temperature: a TPR study with H₂ and CO as reducing agents, *J. Catal.* 225 (2004) 267–277, <https://doi.org/10.1016/j.jcat.2004.04.006>.
- [52] D. Li, N. Ichikuni, S. Shimazu, T. Uematsu, Hydrogenation of CO₂ over sprayed Ru/TiO₂ fine particles and strong metal-support interaction, *Appl. Catal. A Gen.* 180 (1999) 227–235, [https://doi.org/10.1016/S0926-860X\(98\)00335-4](https://doi.org/10.1016/S0926-860X(98)00335-4).
- [53] D.J. Morgan, Resolving ruthenium: XPS studies of common ruthenium materials, *Surf. Interface Anal.* 47 (2015) 1072–1079, <https://doi.org/10.1002/sia.5852>.
- [54] C. Elmasides, D.I. Konardides, W. Gru, X.E. Verykios, XPS and FTIR study of Ru/Al2O3 and Ru/TiO₂ catalysts: reduction characteristics and interaction with a methane–oxygen mixture, *J. Phys. Chem. B* 103 (1999) 5227–5239.
- [55] G. Bergeret, P. Gallezot, Particle size and dispersion measurements, in: G. Ertl, H. Knozinger, J. Weitkamp (Eds.), *Handb. Heterog. Catal.*, 2nd ed., VCH Verlagsgesellschaft mbH, Weinheim, 1997, pp. 439–441, <https://doi.org/10.1002/9783527619474.ch3a>.
- [56] D.D. Sarma, C.N.R. Rao, XPS studies of oxides of second- and third-row transition metals including rare earths, *J. Electron Spectros. Relat. Phenomena* 20 (1980) 25–45, [https://doi.org/10.1016/0368-2048\(80\)85003-1](https://doi.org/10.1016/0368-2048(80)85003-1).
- [57] J.E. Benson, H.W. Kohn, M. Boudart, On the reduction of tungsten trioxide accelerated by platinum and water, *J. Catal.* 5 (1966) 307–313.
- [58] R.B. Levy, M. Boudart, The kinetics and mechanism of spillover, *J. Catal.* 32 (1974) 304–314.
- [59] J. He, C. Zhao, J.A. Lercher, Ni-catalyzed cleavage of aryl ethers in the aqueous phase, *J. Am. Chem. Soc.* 134 (2012) 20768–20775, <https://doi.org/10.1021/ja309915e>.
- [60] J. He, C. Zhao, D. Mei, J.A. Lercher, Mechanisms of selective cleavage of C–O bonds in di-aryl ethers in aqueous phase, *J. Catal.* 309 (2014) 280–290, <https://doi.org/10.1016/j.jcat.2013.09.012>.
- [61] J. He, L. Lu, C. Zhao, D. Mei, J.A. Lercher, Mechanisms of catalytic cleavage of benzyl phenyl ether in aqueous and apolar phases, *J. Catal.* 311 (2014) 41–51, <https://doi.org/10.1016/j.jcat.2013.10.024>.
- [62] J. He, C. Zhao, J.A. Lercher, Impact of solvent for individual steps of phenol hydrodeoxygenation with Pd/C and HZSM-5 as catalysts, *J. Catal.* 309 (2014) 362–375, <https://doi.org/10.1016/j.jcat.2013.09.009>.
- [63] J. Chaminand, L. Djakovich, P. Gallezot, P. Marion, C. Pinel, C. Rosier, Glycerol hydrogenolysis on heterogeneous catalysts, *Green Chem.* 6 (2004) 359–361, <https://doi.org/10.1039/c7gc00620a>.